JGR Atmospheres

RESEARCH ARTICLE
10.1029/2019JD030279

The Influence of Summer Deep Soil Temperature on Early Winter Snow Conditions in Eurasia in the NCEP CFSv2 Simulation

Ravi P. Shukla[1], **Bohua Huang**[1,2], **Paul A. Dirmeyer**[1,2], **and James L. Kinter**[1,2]

[1]Center for Ocean-Land-Atmosphere Studies, George Mason University, Fairfax, VA, USA, [2]Department of Atmospheric, Oceanic, and Earth Sciences, George Mason University, Fairfax, VA, USA

Abstract The National Centers for Environmental Prediction (NCEP) Climate Forecast System version 2 (CFSv2) has a large cold bias in the model's deep soil temperature during summer. This study explores the potential triggering effect of that bias on excessive Eurasian snow cover in early winter. Snow cover appears erroneously early in the fall, especially in western Eurasia, in long simulations with CFSv2. The seasonal transition may be too early because the model land surface temperature (LST) reaches its freezing point earlier than observed, so that new snow cannot melt. This process initiates snow-albedo feedback too early. The early cooling of LST is partially influenced by a seasonal resurfacing of the cold bias in the deep soil layer. From winter to early spring, a cold bias prevails in LST and upper soil temperature as snow cover remains. During this season, the temperature in the deep soil is generally warmer than in the upper soil and has relatively little bias. From spring to summer, the cold bias in the upper soil becomes smaller as it warms up in response to solar heating. On the other hand, the deep soil temperature has a noticeably smaller seasonal change than observed, resulting in a severe cold bias during summer. As the solar radiation declines quickly in early fall, the cold deep soil temperature causes additional cooling in the upper soil layer and helps to bring LST to the freezing point early in the western Eurasia, which leads to enhanced bias in the snow properties.

Key Points:
- Model overestimates SCF up to 60% in western Eurasia during October because LST reaches its freezing point there earlier than observed
- The Model deep soil temperature has a noticeably smaller seasonal change than observed, resulting in a severe cold bias during summer
- Cold deep soil temperature causes additional cooling in upper soil layer and helps to bring LST to freezing point early over there

Supporting Information:
- Supporting Information S1
- Table S1

Correspondence to:
R. P. Shukla,
rshukla2@gmu.edu

Citation:
Shukla, R. P., Huang, B., Dirmeyer, P. A., & Kinter, J. L. (2019). The influence of summer deep soil temperature on early winter snow conditions in Eurasia in the NCEP CFSv2 simulation. *Journal of Geophysical Research: Atmospheres*, *124*, 9062–9077. https://doi.org/10.1029/2019JD030279

Received 9 JAN 2019
Accepted 2 AUG 2019
Accepted article online 9 AUG 2019
Published online 19 AUG 2019

1. Introduction

In recent decades, substantial progress has been made in reproducing the observed mean states and interannual variability in state-of-the-art coupled general circulation models (CGCM) due to advances in atmospheric observing systems, high-end computing resources, and increasingly realistic representations of the interactions between the ocean and atmosphere and the land surface and atmosphere (Wang et al., 2005). However, a number of systematic biases and uncertainties persist in CGCMs, so that seasonal forecasts are not as accurate as they potentially could be. Many previous studies have revealed that land surface conditions, including snow cover, land surface temperature (LST), soil moisture and vegetation influence the evolution of weather patterns and climate variability (e.g., Cohen & Rind, 1991; Dirmeyer, 2005; Koster et al., 2010; Seneviratne et al., 2010; Shukla & Mintz, 1982). Therefore, land-atmosphere interactions have received increasing attention using the CGCMs and observations (e.g., Xue et al., 1991; Roesch, 2006; Dutra et al., 2011; Furtado et al., 2015; He et al., 2016; Li et al., 2016; Dirmeyer & Halder, 2017). In particular, Eurasian snow cover can influence large-scale atmospheric circulation anomalies in the middle and high latitudes of the Northern Hemisphere (e.g., Barnett et al., 1988; Cohen et al., 2007; Foster et al., 1983), the Indian summer monsoon rainfall (e.g., Barnett et al., 1988; Dickson, 1984; Hahn & Shukla, 1976; Halder & Dirmeyer, 2016), and summer rainfall in eastern China (e.g., Yang & Lau, 1998; Yasunari et al., 1991; Zuo et al., 2012).

In contrast, the possible influence of subsurface soil temperature (SUBT) anomalies on climate variability has been less discussed, although a few studies are available (Fan, 2009; Mahanama et al., 2008; Wu & Zhang, 2014; Xue et al., 2012, 2018). The SUBT is an important variable in models that include representations of soil heat storage and transfer. Using an atmospheric general circulation model, Mahanama et al. (2008) conducted experiments with specified SUBT, interactive SUBT, and a prescribed climatological annual cycle of sea surface temperature, showing that interactive SUBT significantly increases surface air temperature variability and memory in most regions. Fan (2009) used observed soil temperature to

initialize a regional land surface climate model and showed that observed soil temperature introduces a persistent soil heating condition that is favorable to convective development and improves the prediction of precipitation. Wu and Zhang (2014) made two long-term regional climate model simulations with and without subsurface soil temperature to investigate the role of soil temperature–atmosphere coupling in influencing the interannual variability of summer climate over East Asia. They found that SUBT feedbacks play an important role in amplifying summer surface air temperature variability over the arid/semiarid regions of the East Asia.

Recently, Xue et al. (2018, 2016, 2012) explored the relationship between spring LST/SUBT anomalies and the summer precipitation anomaly over the contiguous United States and East Asia using the National Centers for Environmental Prediction (NCEP) Global Forecast System and a regional climate model. Using observational data sets, they found significant correlation between summer precipitation and spring LST/SUBT anomalies over the two continents, and they confirmed the relationship between these two variables, suggesting that the long-distance effect of land temperature changes in the northwest United States and the Tibetan Plateau on the respective downstream regions is probably as large as the more familiar effects of sea surface temperature and atmospheric internal variability.

In this paper, we systematically explore the importance of SUBT on snow conditions in the Eurasia in simulations made with the coupled NCEP Climate Forecast System, version 2 (CFSv2; Saha et al., 2014). Many previous studies have used CFSv2 to examine different aspects of the seasonal-to-interannual prediction and interannual variability (Kim et al., 2012; Shukla & Huang, 2015; He et al., 2016; Dirmeyer & Halder, 2017; Shukla et al., 2017; Huang et al., 2017; Broxton et al., 2017, and papers cited therein). For instance, specifically for CFSv2 reforecasts, He et al. (2016) demonstrated that the model reproduces the observed Eurasian snow cover fraction (SCF) climatology and annual cycle. However, they also reported that CFSv2 has worse skill in predicting SCF anomalies during the snowfall season than in the snowmelt season. In another study, He et al. (2018) discussed snow water equivalent (SWE) during March–May (MAM) in Eurasia using CFSv2 reforecasts. They found that CFSv2 reproduces the spatial distribution of SWE at a lead time of 1–3 months. CFSv2 produces excessive snow cover and SWE in Eurasia throughout the winter-spring season, partly due to an overactive snow-albedo feedback. Broxton et al. (2017) found that CFSv2 reforecasts produce systematic differences in SWE and surface air temperature, depending on the forecast lead time. They attributed these biases to errors in the radiative transfer and/or land surface components of the model (e.g., snow parameterizations).

The causes of excessive bias in SCF and SWE over western Eurasia in CFSv2 simulation during October to November remain unclear. In this paper, we examine how the cold bias of SUBT at 100- to 200-cm depth in western Eurasia during July to September in CFSv2 simulations can affect the snow properties (e.g., SCF and SWE) in the following October to December. Our results demonstrate that the freezing temperature (273.15 °K) of LST in the Eurasia advances westward too early in comparison to reanalysis during September to December due to excessively cold anomalies in the SUBT at 100- to 200-cm depth in July to September. We further demonstrate that the excessive snow properties during October to December can affect the mean state of the atmosphere in spring.

The remainder of this paper is organized as follows. Section 2 briefly describes the CFSv2, the experimental design, and verification data sets. Section 3 presents the role of LST in sustaining excessive snow properties (e.g., SCF, SWE, and surface albedo) over western Eurasia during early winter. Section 4 describes the feedback of summer SUBT bias at deep soil layer (100–200 cm) on early winter surface condition over the Eurasia in CFSv2 simulation. A summary and discussion are given in section 5.

2. Model Description, Experimental Design, and Observational Data Sets

The CGCM used in this study is NCEP CFSv2 (Saha et al., 2014), which includes atmospheric, oceanic, sea ice, and land components. It has a spectral horizontal resolution of T126 (105-km grid spacing) and 64 vertical levels in a hybrid sigma pressure coordinate. The subgrid-scale physical parameterization package includes absorption and emission of radiation, cloud formation, and dissipation, including stratus, stratocumulus and cumulus clouds, turbulence in the planetary boundary layer, and a complex formulation of the formation, precipitation, and reevaporation of rainfall. The oceanic component of CFSv2 is the Geophysical Fluid Dynamics Laboratory Modular Ocean Model version 4 (MOM4; Griffies et al., 2004),

which is configured for the global ocean with a horizontal grid of 0.5° × 0.5° poleward of 30°S/30°N and meridional resolution increasing gradually to 0.25° between 10°S and 10°N (nominally referred to as 0.5° resolution). Vertically, it has 40 levels in a z coordinate, with 27 levels within the upper 400 m and the maximum depth at approximately 4.5 km. Recently added features of MOM4 include replacing "virtual salt flux" with real freshwater flux and updated lateral mixing of both tracers and momentum (Gnanadesikan et al., 2006). The sea ice component is a three-layer global interactive dynamical sea ice model with predicted fractional ice cover and thickness (Winton, 2000). The land surface component is the Noah land surface model. Directly coupled to the atmospheric component, the Noah land surface model is a computationally efficient model of intermediate complexity for use in operational weather and seasonal prediction models (Ek et al., 2003).

In this study, we have used a revised version of CFSv2 with adjusted parameters for sea ice albedo to maintain realistic multiyear sea ice cover in the Arctic Ocean as described in Huang et al. (2015). We produced a 50-year simulation, which was initialized from the Climate Forecast System Reanalysis (CFSR; Saha et al., 2010) initial conditions of atmosphere, land, sea ice, and ocean at 00Z, 1 January 1980 with a fixed greenhouse gas (GHG) level for 2,000 (Shukla et al., 2017). Therefore, the simulation is not forced by the observed and projected GHG increase.

The monthly gridded surface temperature, soil temperature (four layers) are used from the CFSR during the period 1979–2008 (Saha et al., 2010). We have also used monthly snow water equivalent (SWE; kg/m^2) from the Global Land Data Assimilation System, version 2.0, (GLDAS-2.0) for 2000–2016 at a resolution of 0.25° latitude by 0.25° longitude (Rodell et al., 2004). Radiation fluxes, SCF, and surface albedo are available from the Clouds and the Earth's Radiant Energy System (Wielicki et al., 1996) Energy Balanced and Filled (CERES-EBAF) data set for the recent period (2001–2015) at 1° × 1° resolution. The surface sensible and latent heat flux data for 1979–2007 are taken from the European Centre for Medium-Range Forecasts Interim Re-Analysis (ERA-Interim; Dee et al., 2011) on the T255 horizontal grid. We have used both the U.S. Air Force snow depth analysis monthly climatology for 1979–1998 at 1° × 1° (Foster & Davy, 1988) and the Rand Corporation mean monthly global snow depth, version-1 (Schultz & Bregman, 1988) in our analysis. Monthly gridded temperature, wind (u,v), and geopotential height (H) at various levels are used from the CFSR. The surface temperature and 2-m temperature are also taken from the ERA 40 reanalysis (Uppala et al., 2005). We have employed monthly means based on the instantaneous prognostic fields at 00Z in both the CFSv2 simulation and CFSR reanalysis (e.g., surface temperature, subsurface soil temperature, and large-scale atmospheric circulation). Table S1 in the supporting information contains details of reanalysis, resolutions, periods, and references related to it.

For this analysis, we have discarded the first 20 years of the simulation as spin-up so a quasi-equilibrium is reached among the model atmosphere, land, and upper ocean, with a stable annual cycle and natural climate variability. We have defined the model climatology from the simulation of the last 30 years (2000–2030). As a free simulation, the model years 2000–2030 have no connection with the real calendar years. This model climatology is compared with the CFSR climatology derived from the assimilation in 1979–2008. Therefore, the CFSR climatology is fully observation-based and in a period with the GHG level comparable to the specified one in the model simulation.

For quantitative model-data comparison, both model and observational fields are interpolated onto a common 1° × 1° grid. We have tested the statistical significance of these bias patterns point-wise using a Student's t test. The biases at most of the dominant centers of action in this paper are statistically significant above the 99% statistical significance level.

3. The Role of LST in Sustaining Excessive Snow Over Eurasia

In this section, first, we discuss characteristic features of the LST (obtained by masking out the ocean points from the skin temperature model output) over Eurasia in CFSR and the long simulation. Figure 1 shows the seasonal mean of LST during September to November (SON), December to February (DJF), March to May (MAM), and June to August (JJA) in the reanalysis (Figures 1a–1d) and corresponding model biases (model minus reanalysis) are given in Figures 1e–1h, respectively. Qualitatively, CFSv2 captures the main spatial distribution of reanalysis LST pattern over the Eurasia, including the LST gradient between western and northeastern Eurasia in all seasons (not shown). Quantitatively, the model demonstrates a large cold LST

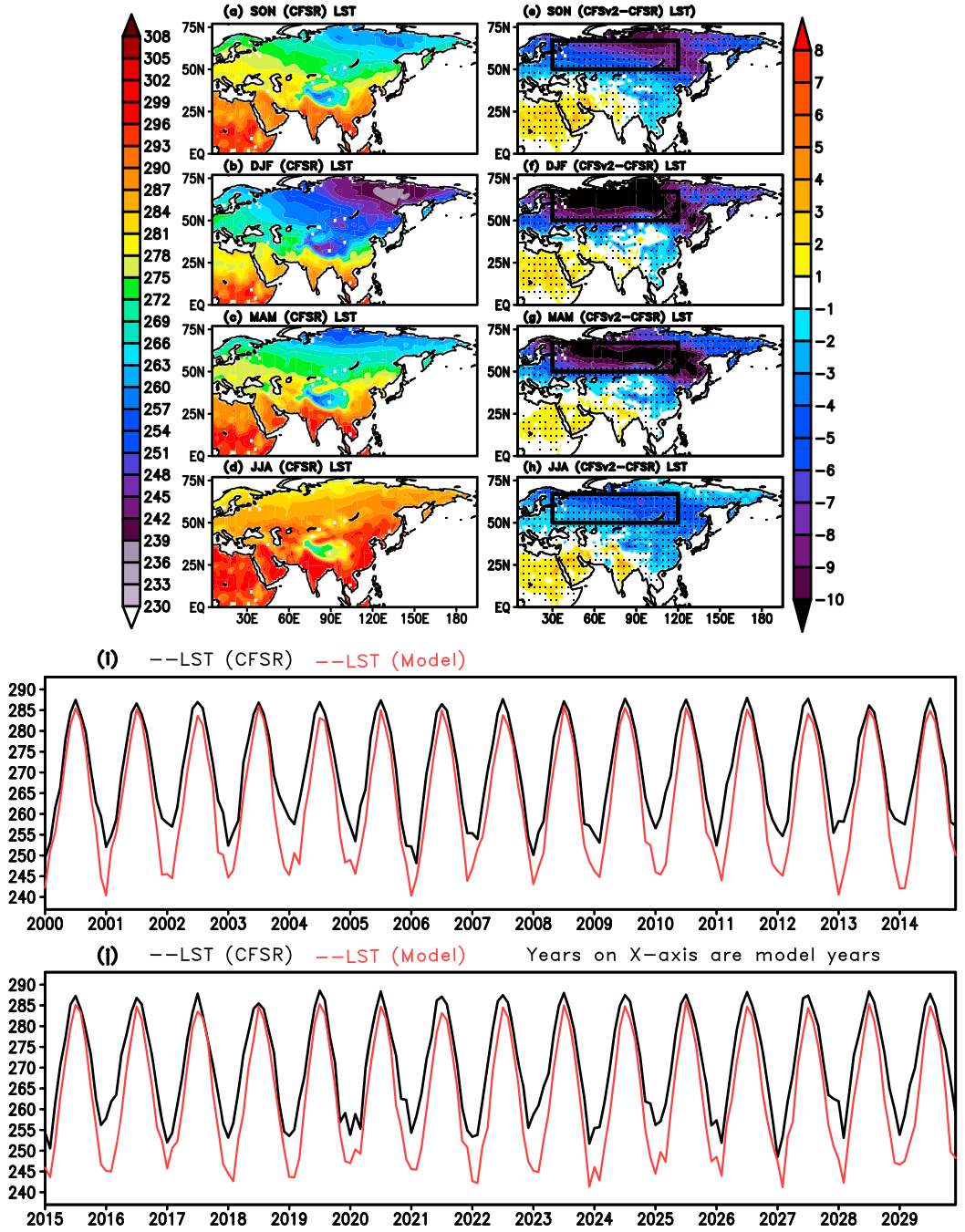

Figure 1. Spatial distribution of the climatological CFSR reanalysis land surface temperature (LST) [degree Kelvin; °K] in (a) SON, (b) DJF, (c) MAM, and (d) JJA. The scale for the magnitude for LST in "°K" is shown at the left of these panels. Spatial distributions of seasonal mean LST biases relative to CFSR in model simulation for (e) JJA, (f) SON, (g) DJF, and (h) MAM. The scale for the magnitude of bias for surface temperature in "°K" is shown at the right of these panels. (i, j) Time series of monthly LST over central Eurasia (box in Figure 1e; domain: 50–67°N, 30–120°E) in 30 years simulation of CFSv2 (red line) and CFSR (black line). Years on *X* axis are model years in (i) and (j). The dotted regions indicate they are statistically significant at 99% confidence level based on a Student's *t* test in (e–h). CFSR = Climate Forecast System Reanalysis; CFSv2 = Climate Forecast System version 2; SON = September to November; DJF = December to February; MAM = March to May; JJA = June to August.

bias of 5–10 °C in most of the Eurasian landmass during all seasons (Figures 1e–1h) but magnitude of cold bias is less (approximately 1–3 °C) in eastern Eurasia (around 70°N) during JJA (Figure 1h). The model depicts excessive cooling of up to 10 °C over central Eurasia during DJF and MAM. Figures 1i and 1j

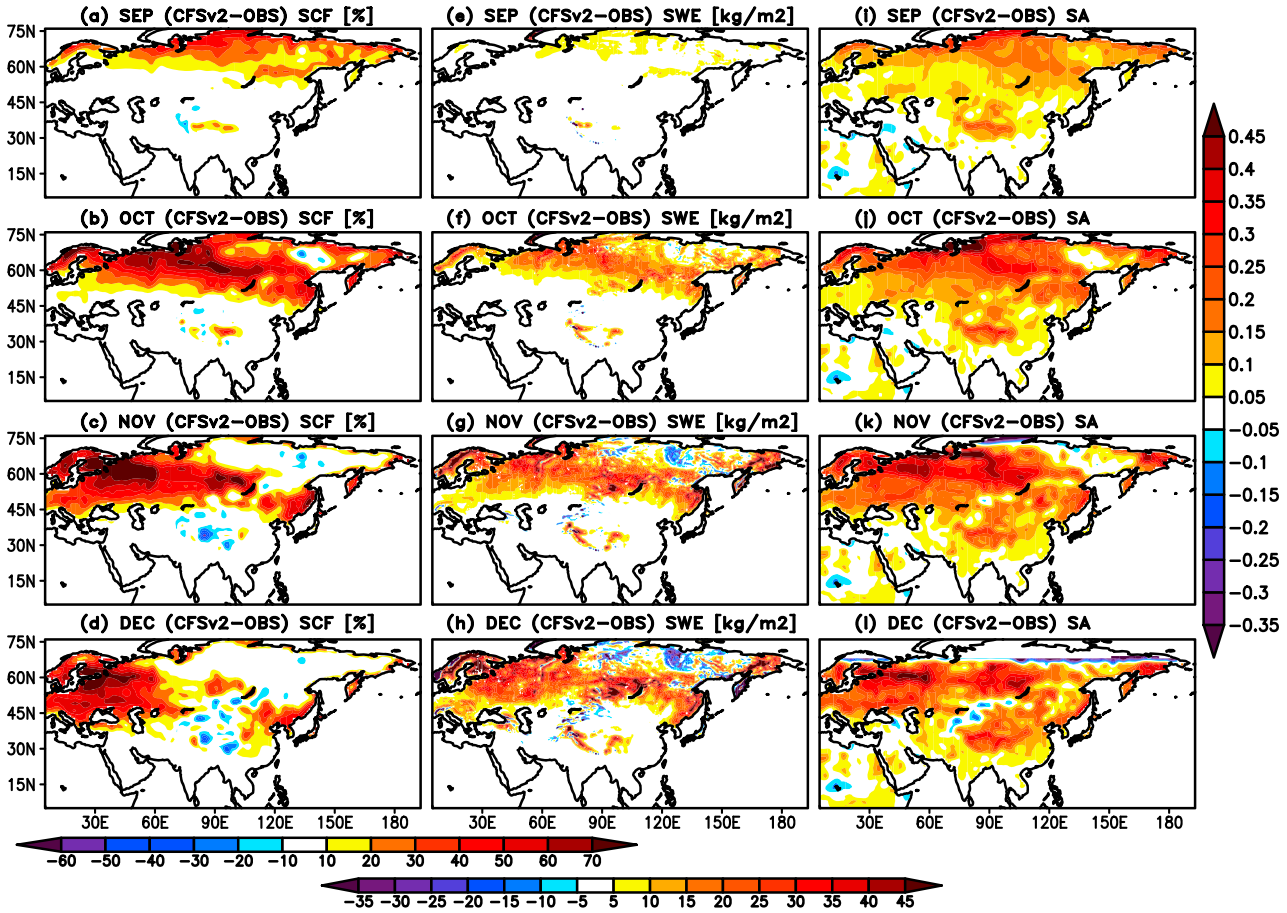

Figure 2. Spatial distributions of monthly snow cover fraction [SCF; %] climatological biases relative to observation in CFSv2 simulation for (a) September, (b) October, (c) November, and (d) December. The scale for the magnitude of bias for SCF in "%" is shown below these panels (first). (e)–(h) As in (a)–(d) but for snow water equivalent [SWE; kg/m^2]. The scale for the magnitude of bias for SWE in "kg/m^2" is shown below these panels (second). (i)–(l) As in (a)–(d) but for surface albedo (SA). The scale for the magnitude of bias for Surface Albedo in "%" is shown at the right of these panels. CFSv2 = Climate Forecast System version 2.

depict the monthly evaluation of an LST index, defined as an area average over central Eurasia (50–67°N, 30–120°E) in CFSR (black line) and the simulation (red line). The phase of the annual cycle of the LST index in the model is in good agreement with CFSR. The magnitude of the annual cycle, however, is too large, with LST index values during peak wintertime being lower in the model simulation than CFSR values by ~12 °K and only 2–3 °K lower during peak summer time. This cold LST bias in Eurasia in CFSv2, which recurs every year, is not due to the influence of initial shock (Shukla et al., 2017) or the initialization time (Shukla et al., 2019), but it is a permanent feature of the model.

Based on observation products and reanalysis (example: Figure S1), stable snow cover in Eurasia is established in October, although some regions (e.g., northeastern Eurasia around 70°N) become snow covered in September. Snowmelt in Eurasia starts in April (not shown). During July and August, there is no evidence of snow in Eurasia in observations (not shown). It is found that the stable SCF in the model simulation is initiated in September; therefore, the model overestimates SCF by up to 20% to 30% in northeastern Eurasia in September (Figure 2a). Quantitatively, the model overestimates SCF up to 60% over the western Eurasia mainly between 55°N to 70°N (Figure 2b) in October. During November and December, the SCF is up to 60% excessive in western Eurasia, mainly in the region 50–70°N, 20–60\°E (Figures 2c and 2d). It is necessary to mention that there is negligible SCF bias in northeastern Eurasia during November and December. The SWE is defined as the amount of water contained within snowpack. It is a prognostic variable in most models. The CFSv2 (not shown) captures the observed development, transition, and mature

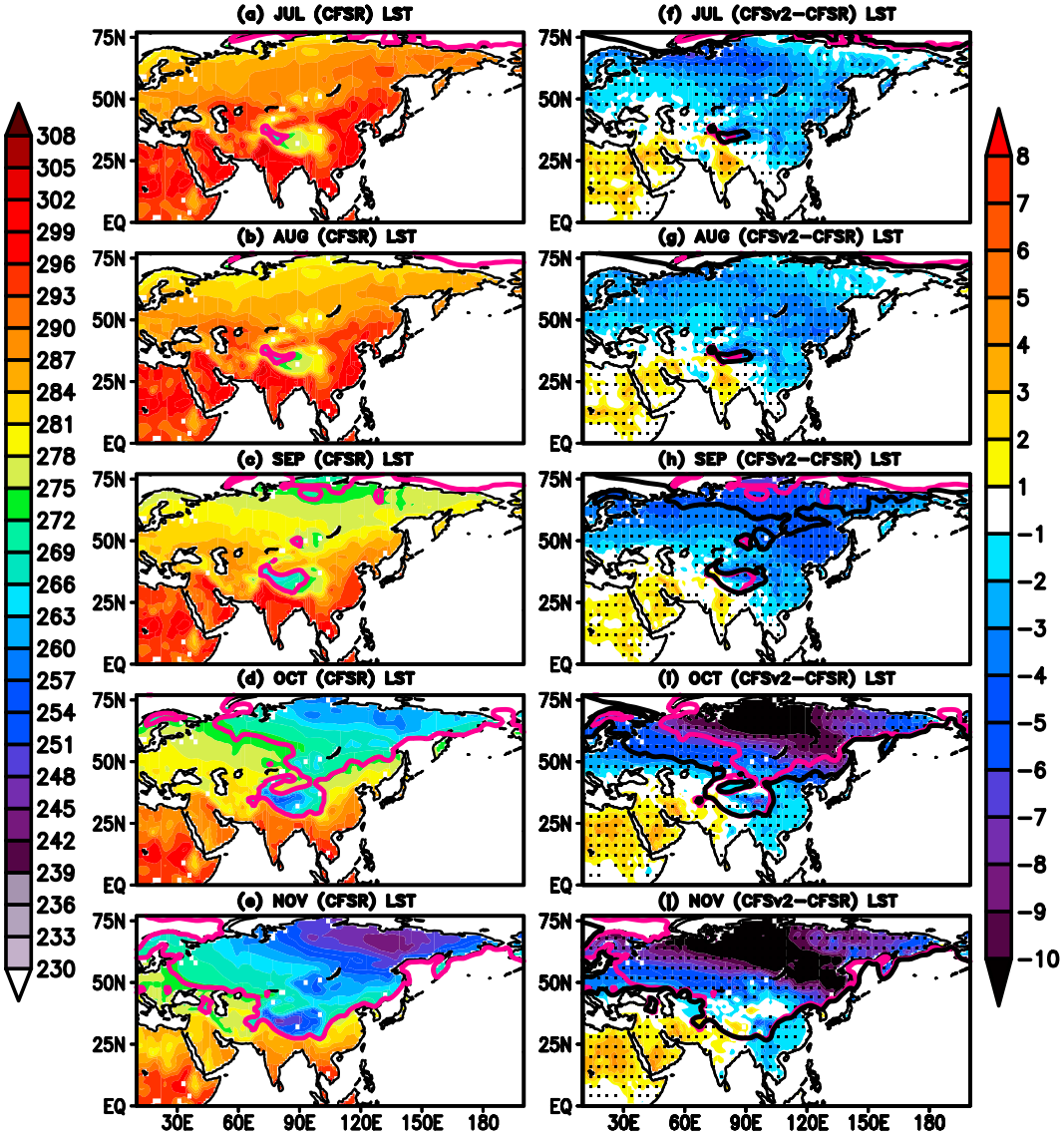

Figure 3. Spatial distribution of the monthly climatological CFSR LST [°K] in (a) July, (b) August, (c) September, (d) October, and (e) November. The scale for the magnitude for LST in "K" is shown at the left of these panels. Spatial distributions of the monthly climatological LST bias relative to CFSR in model simulation for (f) July, (g) August, (h) September, (i) October, and (j) November. The scale for the magnitude of bias for LST in "°K" is shown at the right of these panels. Both red and pink lines in all the panels depict 273.15 °K (freezing temperature) for CFSR (red line) and CFSv2 (black line). The dotted regions indicate they are statistically significant at 99% confidence level based on a Student's *t* test in (f)–(j). CFSR = Climate Forecast System Reanalysis; CFSv2 = Climate Forecast System version 2.

phases of SWE in Eurasia; however, it overestimates SWE (Figures 2f–2h) in western Eurasia during November and December by up to 30 kg/m^2. The positive bias in SWE during October is mainly in northern central Eurasia, which is consistent with the SCF bias there. The model also overestimates snow depth in Eurasia during October to December (not shown). Consistent with the biases of SCF and SWE during October to December, CFSv2 has a large positive bias in surface albedo in the northern western Eurasia up to 0.35 (Figures 2j–2l).

The location of SCF, SWE, and surface albedo biases during September to December shifts westward from month to month. For example, the location of maximum bias in Eurasian SCF shifts from 70°E in October to 50°E in November. This raises a question: What causes the early and excessive snow properties in western Eurasian in October to December?

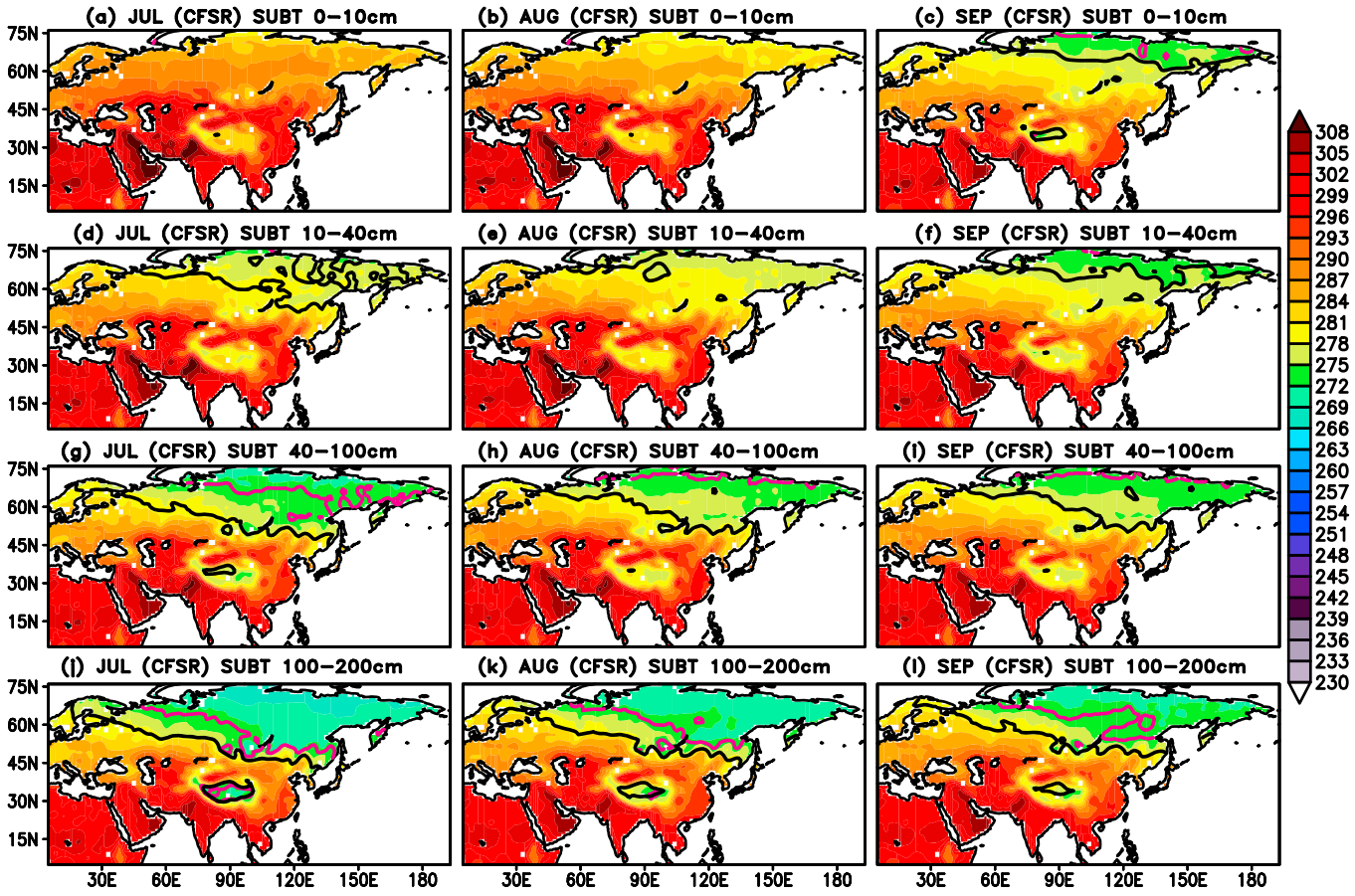

Figure 4. Spatial distribution of the monthly climatological CFSR subsurface soil temperature (SUBT) at 0–10 cm [°K] in (a) July, (b) August, and (c) September. The scale for the magnitude for SUBT in "°K" is shown at the right of these panels. The red line in Figures 4a–4c denotes 273.15 °K in CFSR SUBT at 0–10 cm. The black line in Figures 4a–4c denotes 273.15 °K in the simulation of CFSv2 SUBT at 0–10 cm. (d)–(f) As in (a)–(c) but for SUBT at 10–40 cm. (g)–(i) As in (a)–(c) but for SUBT at 40–100 cm. (j)–(l) As in (a)–(c) but for SUBT at 100–200 cm. CFSR = Climate Forecast System Reanalysis.

To answer this question, we first consider monthly mean LST in CFSR (Figures 3a–3e) and the corresponding biases (model-CFSR; Figures 3f–3j) during July to November. We have also indicated the freezing temperature (273.15 °K) in CFSR (pink line) and model simulation (black line) in Figures 3a–3j. The model simulation is able to capture the annual cycle of LST in Eurasia, but it underestimates the LST by 4–10 °C, mainly in 45°N to 75°N except in northeastern Eurasia during July and August where there is a warm bias that apparently originates from the oceanic domain further east (not shown).

During August, the freezing temperature (273.15 °K) in Eurasia in both CFSR and the CFSv2 simulation (Figure 3g) is located at almost the same place, mainly at 75°N. A dramatic feature of the CFSv2 simulation (Figure 3h) is that the freezing line moves more quickly southwestward toward western Eurasia from August to September than in CFSR (Figure 3g). In October (Figure 3i), the model LST freezing temperature extends to 30°E in western Eurasia, whereas in CFSR it reaches only 60°E. Our results demonstrated (Figure 2) that the model overestimated SCF earlier during early winter, especially in western Eurasia in comparison to observations. A possible explanation of the overestimated SCF in early winter is that the LST reaches the freezing point over western Eurasia earlier in the simulation than in the observed, so that new snow falling on the frozen ground cannot melt. This process initiates the snow-albedo feedback too early in the season, which enhances the bias in snow properties in western Eurasia.

In addition to CFSR, we have also calculated the biases of the model LST and 2-m temperature using the ERA40 reanalysis. It is found that the spatial structures of biases in these variables are similar with respect to both ERA40 reanalysis (Figures S3–S5) and CFSR (Figures 1a–1h, 3a–3j, and S2), respectively.

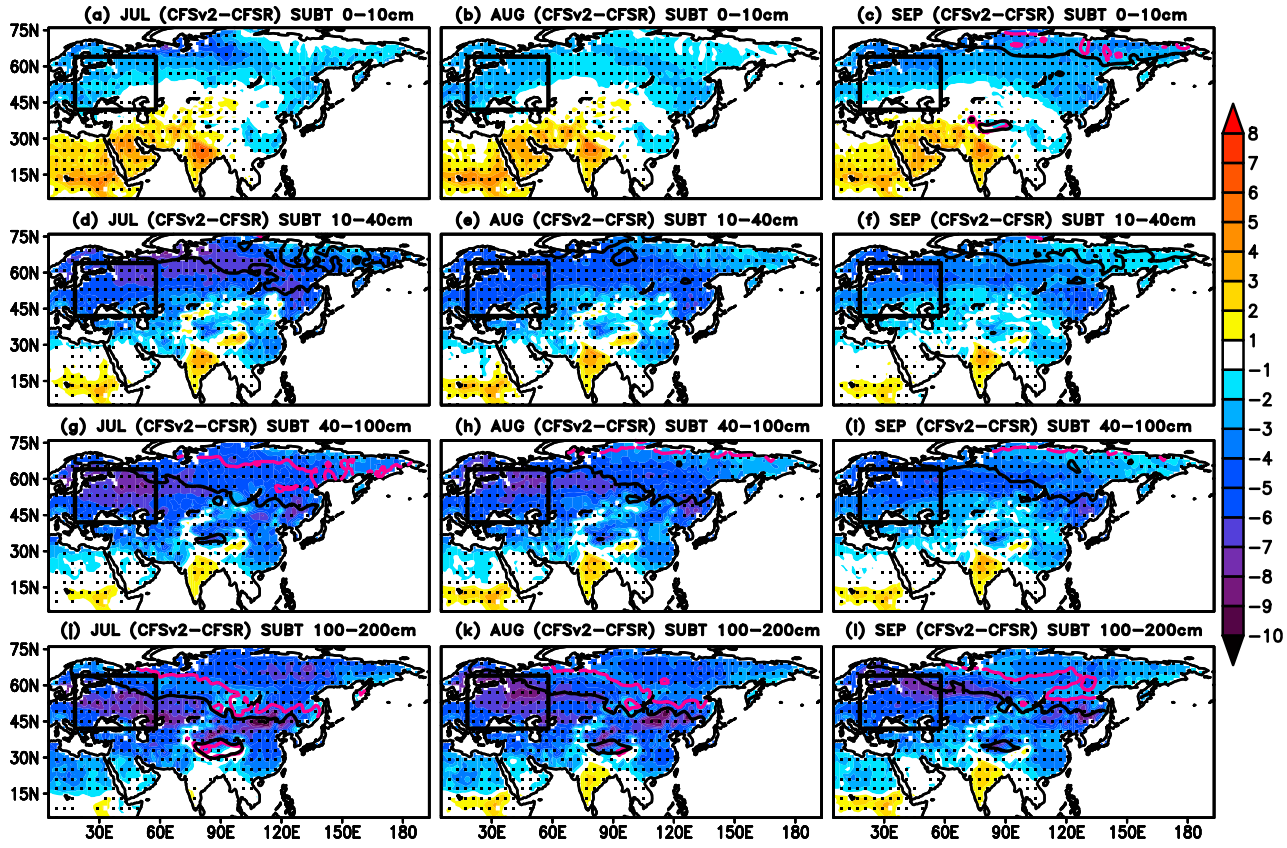

Figure 5. Spatial distributions of monthly SUBT at 0–10 cm climatological biases relative to CFSR in CFSv2 simulation for (a) July, (b) August, and (c) September. The scale for the magnitude for SUBT bias in "°K" is shown at the right of these panels. The red line (black line) in Figures 4a–4c denotes 273.15 °K in CFSR (CFSv2 simulation) SUBT at 0–10 cm. (d)–(e) As in (a)–(c) but for SUBT at 10–40 cm. (g)–(i) As in (a)–(c) but for SUBT at 40–100 cm. (j)-(l) as in (a)-(c) but for SUBT at 100-200cm. The dotted regions indicate the statistically significant at 99% confidence level based on a Student's *t* test. CFSR = Climate Forecast System Reanalysis; CFSv2 = Climate Forecast System version 2; SUBT = subsurface soil temperature.

In the next section, the origin of early freezing will be explored.

4. Bias of Deep-Layer Soil Temperature in Eurasia

The climatological mean SUBT behaves somewhat differently at different depths. The monthly climatology of SUBT during July to September is shown in Figure 4 for CFSR and Figure 5 for the CFSv2 simulation biases: 0–10 cm in Figures 4a–4c and 5a–5c, 10–40 cm in Figures 4d-4f and 5d–5f, 40–100 cm in Figures 4g–4i and 5g–5i, and 100–200 cm in Figures 4j–4l and 5j–5l. A strong meridional gradient between western Eurasia around 55°N and northeastern Eurasia around 65°N occurs in CFSR during July–September at all levels and eastern Eurasia is much cooler than western Eurasia in all SUBT layers (Figure 4). The model simulation reproduces the SUBT contrast between eastern and western Eurasia at all four levels (not shown). From winter to early spring, the climatological SUBT at 0–10 cm and 10–40 cm resembles LST in Eurasia, sustaining an annual cycle. Consistent with the tendency of LST freezing point in the simulation, the model freezing temperature at 0–10 cm (Figure 4b and 4c) and 10–40 cm (Figure 4e and 4f) more quickly moves from 73°N in August to 65°N in September than reanalysis. The location of the freezing line at 40–100 cm during August and September is in central Eurasia in the model, while it is located around 75°N in CFSR. It is found that the freezing temperature line in Eurasia at 100–200 cm in the simulation (black line; Figures 4j–4l and S6m–S6o) is always located southwestward of the reanalysis position (red line; Figures 4j–4l and S6m–S6o).

The model depicts large cold LST bias during April to June (Figures S6a–S6c) due to overestimate of SCF over central Eurasia; therefore, the model demonstrates large cold bias at upper soil temperature (0–10 cm) over

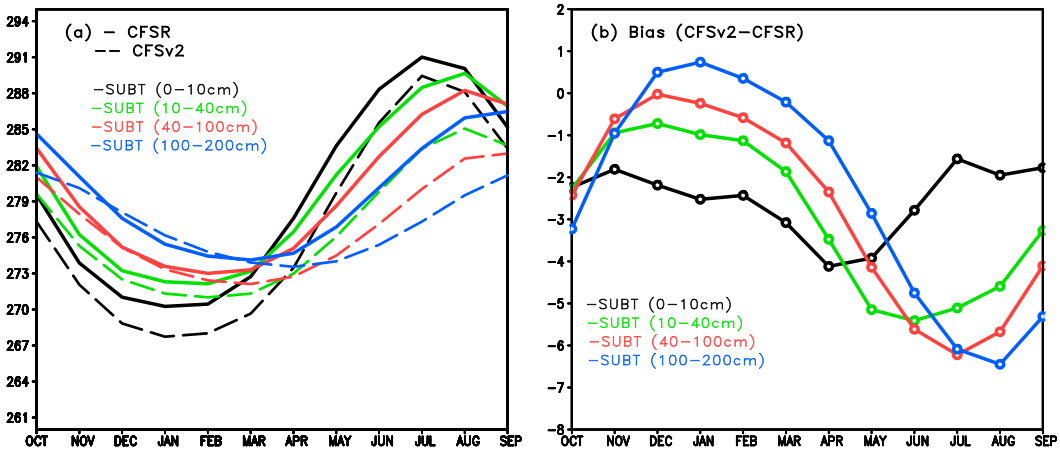

Figure 6. (a) The area averaged monthly climatological SUBT over the western Eurasian (outlined by black box in Figure 5; 42–64°N, 18¯58°E) at 0–10 cm (black line), 10–40 cm (green line), 40–100 cm (red), and 100–200 cm (blue). The solid line indicates for CFSR and long dash line indicates for CFSv2 simulation. (b) The area average of climatological bias between CFSv2 and CFSR over the western Eurasian (CFSv2-CFSR; outlined by black box in Figure 5) for 0–10 cm (black line), 10–40 cm (green line), 40–100 cm (red line), and 100–200 cm (blue line). SUBT = subsurface soil temperature; CFSR = Climate Forecast System Reanalysis; CFSv2 = Climate Forecast System version 2.

there (Figures S6d–S6f). During this period, the deep soil temperature (100–200 cm) shows little bias in model simulation (Figures S6m and S6n). During July–September, the model depicts less cold bias in SUBT at 0–10 cm (Figures 5a–5c) up to 2°K over the Eurasia as the upper layer soil warms up in response to solar heating. The model SUBT at 100–200 cm has a noticeably smaller seasonal change than in reanalysis, resulting in a severe cold bias during summer. The magnitude of cold deep soil temperature bias over western Eurasia is huge during August–September up to 6–7 °K (Figures 5j–5l) in comparison to the upper soil temperature (0–10 cm; Figures 5a–5c) up to 2 °K. The freezing temperature line in the deep soil layer in the model simulation is located near the maximum cold bias in western Eurasia during summer. As the solar radiation reduces quickly in the early fall, the cold SUBT bias at 100–200 cm in western Eurasia during July–September causes additional cooling of the upper soil layer and helps to bring LST to the freezing point early (Figure 7), which provides a favorable condition for excessive snow cover (Figure 2) in the subsequent October to November over there. Because of the large cold bias in the model's deep soil temperature during summer in western Eurasia, the simulated freezing temperature line in LST (Figure 3) during September to November is located west in comparison to its location in CFSR (pink line). Our results demonstrate that the large cold bias in the model's deep soil temperature during summer provides a favorable environment for excessive SCF, SWE, and surface albedo in early winter.

To quantify the variation of annual cycle of soil temperature over western Eurasia, Figure 6a shows the area-averaged climatological SUBT (outlined by the black box in Figure 5: 42–64°N, 18–58°E) at 0–10, 10–40, 40–100, and 100–200cm for CFSR and the model simulation, and the corresponding differences are displayed in Figure 6b. During winter (summer), solar radiation decreases (increases) thereby cooling (warming) the upper soil temperature at 0–10 cm, with a minimum (maximum) value of SUBT at 0–10 cm in western Eurasia of 270.3 °K (291.7 °K) in CFSR and 267.2 °K (289.0 °K) in the simulation. The temporal variation and range of SUBT at 0–10 cm in the simulation are similar to those in CFSR. The minimum (maximum) value of SUBT at 100–200 cm is 273.9 °K (285.9 °K) for CFSR and 273.1 °K (280.6 °K) for the simulation. The difference between the maximum and minimum SUBT is 7.5 in the simulation and 12.0 in CFSR, that is, the range of climatological variations of SUBT at 100–200 cm in the simulation is weaker in comparison to CFSR. There is at least a 1-month phase lagged in annual cycle of deep soil temperature in model in comparison to CFSR. Quantitatively, the model has a severe cold bias of up to 6 °K in the deep soil temperature at 100–200 cm during July to September, compared to a bias of 2 °K for the upper soil layer (Figure 6b).

To further explore the potential effect of the large summer cold bias in the model's deep soil temperature on early winter surface conditions, we have selected an extreme cold year and an extreme warm year based on the normalized interannual time series of July to September mean (JAS) SUBT at 100–200 cm in western

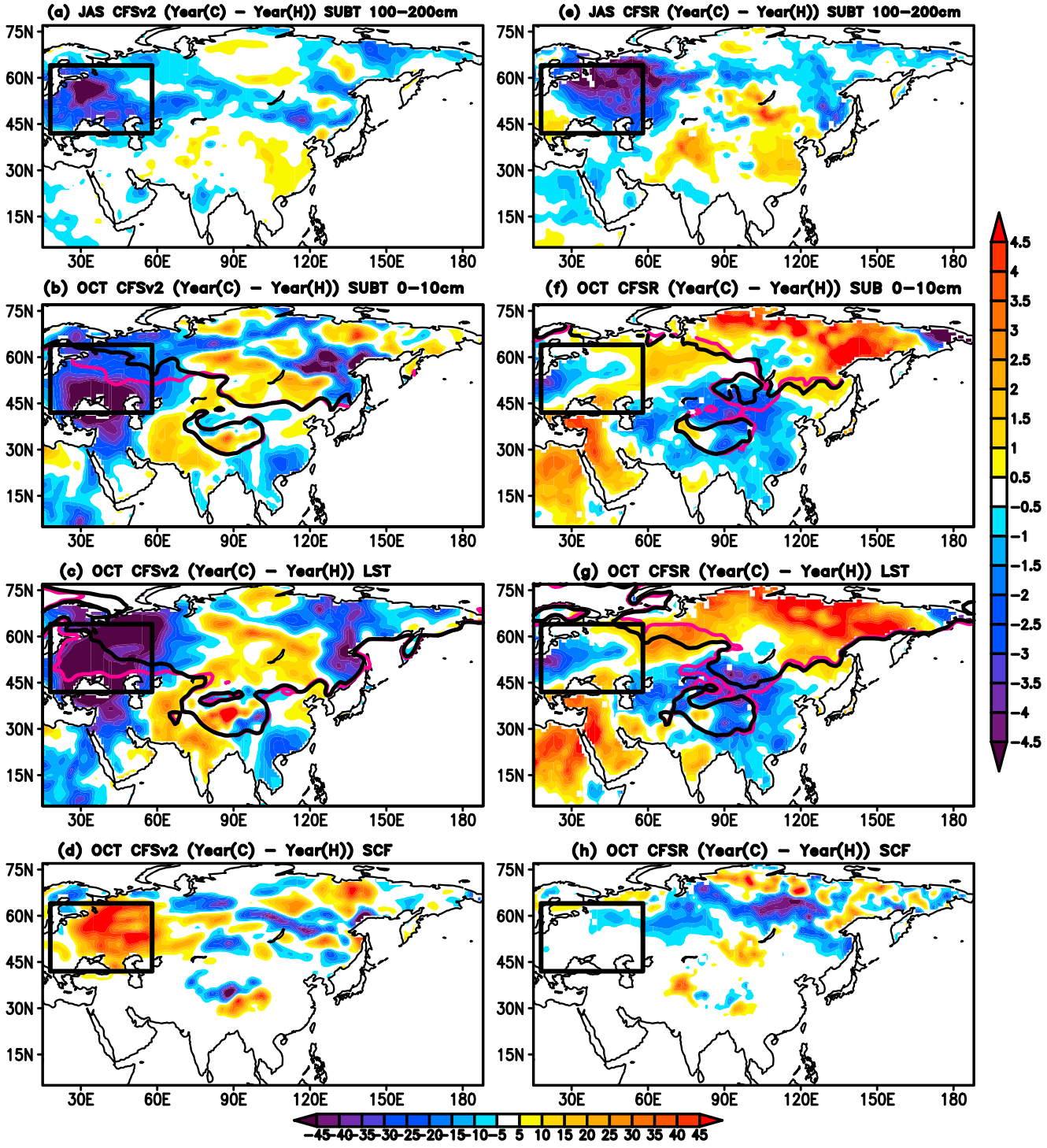

Figure 7. Difference between an extreme cold year and warm year of SUBT at 100–200 cm over the western Eurasian (outlined by black box in Figure 7; 42–64°N, 18–58°E) during July to September mean (JAS) in the CFSv2 simulation. (b) As in (a) SUBT at 0–10 cm during October. The red line (black line) in Figure 7b denotes 273.15°K in cold year (warm year) in CFSv2. (c) As in (a) but for LST during October. The red line (black line) in Figure 7c denotes 273.15°K in cold year (warm year) in CFSv2. (d) As in (a) but for SCF during October. (e)–(h) As in (a)–(d) but for CFSR reanalysis respectively. SUBT = subsurface soil temperature; LST = land surface temperature;SCF = snow cover fraction; CFSR = Climate Forecast System Reanalysis; CFSv2 = Climate Forecast System version 2.

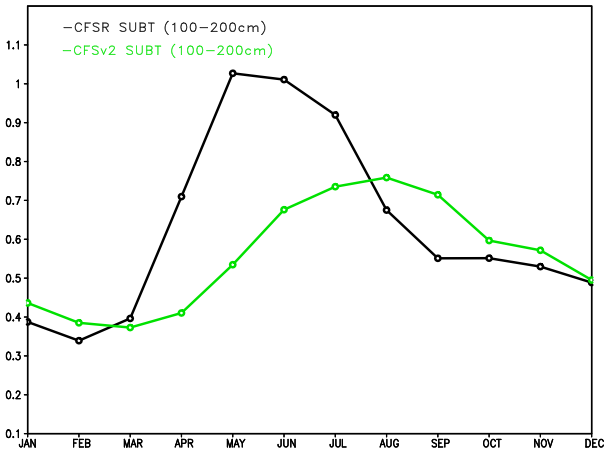

Figure 8. Annual cycle of the standard deviations of monthly anomalies of the SUBT index at 100–200 cm for CFSR (black line) and CFSv2 simulation (green line). SUBT = subsurface soil temperature; CFSR = Climate Forecast System Reanalysis; CFSv2 = Climate Forecast System version 2.

Eurasia (area average over the black box in Figure 5; 42–64°N, 18–58°E). Figure 7a displays the difference of simulated JAS deep soil temperature between the extreme cold and warm years, while Figures 7b–7d show the difference between same cold and warm years for SUBT at 0–10 cm, LST, and SCF during the following October. The difference in deep soil temperature between cold and warm years depicts a large cooling over western Eurasia during JAS (Figure 7a). The enhanced cooling in SUBT 0–10 cm (Figure 7b) and LST (Figure 7c) is found in the following October. The influence of summer deep soil temperature on the subsequent October SUBT 0–10 cm and LST is shown by the location of the freezing temperature line in the cold year (pink color) relative to the warm year (black color) in the simulation (Figures 7b and 7c). The simulated freezing line during October in the cold year is located southwestward of its location in the warm year. There is also a large difference in SCF in western Eurasia between cold and warm years (Figure 7d). Using the same analysis on CFSR does not show the same relationship (Figure 7e–7h). An analogous composite analysis using the mean of five cold versus five warm years from the simulation and from CFSR produces a similar result (Figure S7).

Our further analysis demonstrates that the simulated deep soil temperature in western Eurasia is not as strongly phase-locked to the annual cycle as in CFSR, as shown by the annual cycle of the interannual standard deviation (ISD) of the SUBT 100–200 cm index (Figure 8). The annual cycle of ISD in CFSR at 100–200 cm has a maximum value (1.00) in May and a minimum value (0.35) in February, indicating a strong phase locking to the annual cycle (Figure 8, black line). We have used standard procedures to generate anomalies for each month to calculate ISD. For example, for January case, the climatology for January is removed to generate SUBT anomalies at deep soil SUBT (100–200 cm). There is a sharp transition from March to April and April to May in CFSR. The model simulation is able to reproduce the shape of the monthly ISD of SUBT at 100–200 cm with a high value (0.72) in August and minimum value (0.40) in February (Figure 8, green line). The model does not produce a sharp transition of ISD from March to April and the peak variability is shifted to August. Because deep SUBT at 100–200 cm is not strongly phase-locked in the simulation, some deep soil temperature events may persist longer.

We have calculated the climatological differences between SUBT at 100–200 cm and SUBT at 0–10 cm in both CFSR (Figures 9a–9f) and the model simulation (not shown) during May to October. From May to September (Figures 9a–9e), heat is generally transferred downward within the soil, especially to the north of 50°N, because the deep layer is colder than the upper layer. The direction of heat transfer is reversed in October (Figure 9f), as the upper layer becomes colder than the deep one. The corresponding model biases during this period are given in Figures 9g–9l. In May (Figure 9g) and June (Figure 9h), the model temperature difference is smaller than that in CFSR to the north of 50°N, because the model surface temperature is colder in spring as a result of lingering snow cover. From July to September (Figures 9i–9k), the model has negative biases in the soil temperature difference between the deep and upper layers over the western Eurasia. The negative downward temperature gradient is stronger in the model simulation than in CFSR. Therefore, from summer to early fall, the model top soil layer loses more heat to the deeper layer in the simulation than in CFSR.

To further explore the heat balance of the top layer of soil during this period, we have also calculated the net heat exchange at the land surface over Eurasia. Following Shukla et al. (2019), the net surface heat flux is defined as the difference between the downward radiation flux (sum of downward shortwave radiation [SWR] and longwave radiation [LWR]) and the upward heat flux (the sum of upward SWR and LWR, as well as the surface sensible heat flux [SHF] and surface latent heat flux into the atmosphere) Figures 9m–9r show the climatological biases of net surface heat flux (positive downward) during May to October. The land surface is generally gaining more heat from the atmosphere in the model simulation than in CFSR over most of Eurasia from 25°N to 60°N from May to August. This is mainly caused by excessive solar radiation reaching the land surface due to inadequate cloud cover. This seems to compensate the heat loss from the upper soil

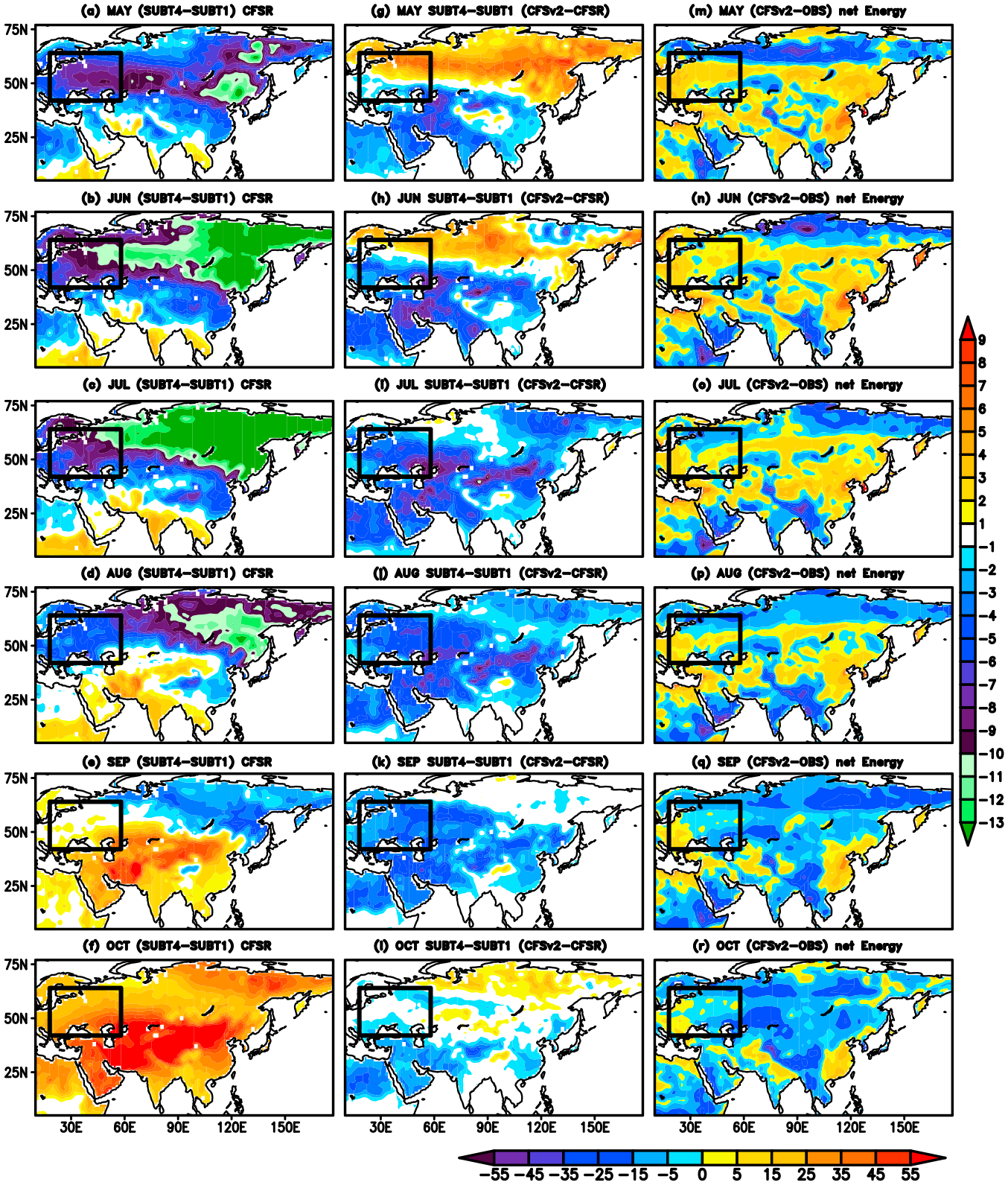

Figure 9. (a)–(f) Spatial distribution of the climatological difference between subsurface temperature (SUBT) at 100–200 cm and SUBT 0–10 cm in Climate Forecast System Reanalysis (CFSR) from May to October. The corresponding model biases are given in Figures 9g–9l. Spatial distributions of monthly net-energy-at-surface climatological biases relative to observation in model simulation during May to October are shown in Figures 9m–9r.

layer to the deeper layer during these months. As the net surface heat flux becomes negative in September at the same time that heat is transferred from the upper to deep soil layers, a rapid cooling of the top soil layer is expected.

Figure S8 in the supporting information displays the climatological bias of surface SHF (Figures S8a–S8f), net LWR (Figures S8g–S8l) and net SWR (Figures S8m-S8r) during May to October. It is also found that the model has negative surface SHF (Figures S8b–S8e) bias during June to September over northwestern Eurasia (outlined by black box in Figures S8b–S8e; 42–64°N, 18¯58°E). The bias in surface SHF (Figures S8b–S8e) over western Eurasia may be related to the large negative bias over western Eurasia in the difference between SUBT at 100–200 cm and SUBT at 0–10 cm during June to September (Figures 9h–9k). During May and June, the model has a large negative bias of net energy over the northern Eurasia, mainly between 60–70°N, which may be related to the bias in surface SHF (Figures S8a and S8b) and net SWR (Figures S8m and S8n). The cause of net SWR bias is mainly the excessive snow cover area and surface albedo biases in Eurasia. The bias in surface SHF is mainly due to the large negative bias in LST during May and June.

Several previous studies demonstrated that autumn snow anomalies over Eurasia could influence the following winter surface temperature and atmospheric circulation (e.g., Jhun & Lee 2004). We have found excessive snow cover in October to December in western Eurasia in the model simulation due to the influence of a large cold bias in the model's deep soil temperature during summer. It may be possible that the enhanced SCF anomalies in late fall can decrease the LST in the following winter. Our previous analysis (Shukla et al., 2019) of the CFSv2 seasonal reforecasts demonstrated that the reforecast runs initialized in February produce excessive snow cover and snow amount in Eurasia throughout the spring season due to an overactive snow-albedo feedback. As a result, the reforecast runs initialized in February produce colder temperatures at the surface and lower troposphere due to reflection of shortwave radiation over erroneously snow-covered areas of Eurasia during spring. Due to this temperature bias (from surface to 600 hPa), the geopotential heights in the middle to upper troposphere are generally 40 to 60 m lower in the CFSv2 reforecasts over middle and high latitudes, which in turn contribute to a large-scale atmospheric circulation bias at 200 Pa. In the current study, we have performed similar analysis using 30 years of CFSv2 simulations and produced consistent results (Figure S9). Therefore, the focus of this study is to examine the potential root causes that generates the seasonal biases in both reforecasts and long-term simulations.

This study may provide further insight into the mechanisms for influence of the land thermal condition on Eurasian climate, especially the Asian monsoon. Hahn and Shukla (1976) reported that a positive (negative) anomaly of snow cover over Eurasia during winter or spring is followed by an anomalous weak (strong) monsoon during the subsequent summer. Since the pioneering work by Hahn and Shukla (1976), many others demonstrated that the Eurasian winter/spring snow cover condition and snow depth influences interannual variability of the succeeding Asian summer monsoon (Bamzai & Shukla, 1999; Barnett et al., 1988; Dickson, 1984; Halder & Dirmeyer, 2016; Kripalani & Kulkarni, 1999; Parthasarathy & Yang, 1995, and others). Some studies (e.g., Zuo et al., 2012) also found that decreasing Eurasian snow cover in spring is significantly associated with reduced precipitation in southeastern China. Wu et al. (2009) reported the impact of spring Eurasia snow cover on decadal variability of summer rainfall over eastern China. The recent study by Shukla et al. (2019) and the results of this study further suggest that the land surface and subsurface thermal condition may play roles in preconditioning and enhancing the snow influence on regional climate.

We have also examined the climatological bias of LST in CGCMs from the Coupled Model Intercomparison Project phase 5 (CMIP5; Taylor et al., 2012) historical simulations from September to November over the Eurasia. Our results suggest that the LST cold bias during fall can also occur in other major climate systems but is not a universal problem. We have not been able to analyze SUBT from these CMIP5 simulations because the necessary data are not available.

5. Summary and Discussion

This study investigates the potential influence of subsurface soil temperature anomalies during summer in western Eurasia on the excessive snow in a state-of-the-art coupled model simulation. We have employed a 30-year simulation of an updated version of the coupled CFSv2 for the analysis. The CFSv2 simulation has a cold LST bias in Eurasia during all seasons but the magnitude of the bias is large, up to 10 °C, during DJF and

MAM. The LST biases over Eurasia are not due to the initialization of the simulation or the impact of initial shock in the coupled model; it is a characteristic behavior of the CFSv2.

The model produces excessive snow cover in Eurasia throughout the winter-spring season, partly due to an overactive snow-albedo feedback. The CFSv2 largely overestimated SCF in the early winter by up to 60% in western Eurasia mainly between 50°N and 70°N, while the SCF bias in northeastern Eurasia is negligible. The location of the cold bias shifts westward in western Eurasia between October and November. The early seasonal transition is possibly because the model LST reaches its freezing point in western Eurasia earlier than the observed so that new snow falling on the frozen ground cannot melt and the snow-albedo feedback occurs earlier in the simulation than observed.

One possible cause for excessive snow cover during early winter in western Eurasia in the simulation is the cold deep soil (100–200 cm) anomalies during summer. The model has a large cold bias in the upper SUBT 0–10 cm during winter to early spring due to the cold bias in LST caused by excessive snow cover, while the deep soil has relatively little bias during this period. The simulation has less cold bias during summer (July to September) than in spring in western Eurasia in the SUBT at 0–10 cm due to solar heating of the upper layer. On the other hand, the magnitude of deep SUBT biases during summer is up to 7 °K, because the simulated deep soil temperature has a smaller annual cycle than the observed. As the solar radiation decreases quickly in the early fall, the large deep soil temperature cold bias in western Eurasia causes additional cooling in the upper soil layer that helps to bring LST to the freezing point early, which provides a favorable condition for excessive snow properties in the subsequent October to November. The month-by-month variations of simulated SUBT at 100–200 cm in western Eurasia also reflect at least a 1-month delay relative to the reanalysis. The location of the simulated freezing line in western Eurasia in October during cold years is located southward of the location in warm years. The simulated deep soil temperature in western Eurasia is not strongly phase-locked to the annual cycle as in the reanalysis, which suggests that some deep soil events may persist longer in the model.

These findings have revealed a possible influence of the Eurasian deep soil temperature in summer on the snow properties and other climatic conditions in the subsequent winter. The results of this paper provide direction for further development of the coupled model to improve the representation of the mean state in the Asian monsoon region.

Conflict of Interest

The authors declare that they have no conflict of interest.

Acknowledgments
Funding for this research work was provided by grants from the National Science Foundation (1338427), the National Oceanic and Atmospheric Administration (NA14OAR4310160), and the National Aeronautics and Space Administration (NNX14AM19G). This research is also supported by a grant from the National Monsoon Mission, Ministry of Earth Sciences, Government of India (MM/SERP/COLA-GMU_USA/2013/INT-2/002). The computations were made on the Extreme Science and Engineering Discovery Environment (XSEDE) high-performance computing platform (Towns et al., 2014), and the computational resources are gratefully acknowledged. The authors are grateful to three anonymous reviewers for their constructive comments and suggestions, which improved the quality of the manuscript significantly. The output data from model integrations described here are available from George Mason University upon request. The CFSR, CERES-EBAF, ERA-interim, GLDAS-2.0, ERA40, and Rand Corporation Monthly Global Snow Depth Climatology were obtained from https://climatedataguide.ucar.edu/climate-data/climate-forecast-system-reanalysis-cfsr, https://ceres.larc.nasa.gov/products.php?product=EBAF-TOA, https://www.ecmwf.int/en/forecasts/datasets/reanalysis-datasets/era-interim, https://disc.gsfc.nasa.gov/information/news?title=GLDAS%20Version%202.0%20data%20sets%20released%20by%20NASA%20GES%20DISC, https://apps.ecmwf.int/datasets/data/era40-daily/levtype=sfc/, and https://catalog.data.gov/dataset/rand-corporation-mean-monthly-global-snow-depth, respectively.

References

Bamzai, A. S., & Shukla, J. (1999). Relation between Eurasian snow cover, snow depth, and the Indian summer monsoon: An observational study. *Journal of Climate*, *12*(10), 3117–3132. https://doi.org/10.1175/1520-0442(1999)012<3117:RBESCS>2.0.CO;2

Barnett, T. P., Dumenil, L., Schlese, U., & Roeckner, E. (1988). The effect of Eurasian snow cover on global climate. *Science*, *239*(4839), 504–507. https://doi.org/10.1126/science.239.4839.504

Broxton, P. D., Zeng, X., & Dawson, N. (2017). The impact of a low bias in snow water equivalent initialization on CFS seasonal forecasts. *Journal of Climate*, *30*(21), 8657–8671. https://doi.org/10.1175/JCLI-D-17-0072.1

Cohen, J., Barlow, M., Kushner, P. J., & Saito, K. (2007). Stratosphere-troposphere coupling and links with Eurasian land surface variability. *Journal of Climate*, *20*, 5335–5343.

Cohen, J., & Rind, D. (1991). The effect of snow cover on the climate. *Journal of Climate*, *7*, 689–706.

Dee, D. P., Uppala, S. M., Simmons, A. J., Berrisford, P., Poli, P., Kobayashi, S., et al. (2011). The ERA-Interim reanalysis: Configuration and performance of the data assimilation system. *Quarterly Journal of the Royal Meteorological Society*, *137*(656), 553–597. https://doi.org/10.1002/qj.828

Dickson, R. R. (1984). Eurasian snow cover versus Indian monsoon rainfall—An extension of the Hahn-Shukla results. *Journal of Climate and Applied Meteorology*, *23*(1), 171–173. https://doi.org/10.1175/1520-0450(1984)023<0171:ESCVIM>2.0.CO;2

Dirmeyer, P. A. (2005). The land surface contribution to boreal summer season predictability. *Journal of Hydrometeorology*, *6*(5), 618–632. https://doi.org/10.1175/JHM444.1

Dirmeyer, P. A., & Halder, S. (2017). Application of the land-atmosphere coupling paradigm to the operational Coupled Forecast System (CFSv2). *Journal of Hydrometeorology*, *18*(1), 85–108. https://doi.org/10.1175/JHM-D-16-0064.1

Dutra, E., Schär, C., Viterbo, P., & Miranda, P. M. A. (2011). Land-atmosphere coupling associated with snow cover. *Geophysical Research Letters*, *38*, L15707. https://doi.org/10.1029/2011GL048435

Ek, M. B., Mitchell, K. E., Lin, Y., Rogers, E., Grunmann, P., Koren, V., et al. (2003). Implementation of Noah land-surface model advances in the NCEP operational mesoscale Eta model. *Journal of Geophysical Research*, *108*(D22), 8851. https://doi.org/10.1029/2002JD003296

Fan, X. (2009). Impacts of soil heating condition on precipitation simulations in the Weather Research and Forecasting model. *Monthly Weather Review*, *137*(7), 2263–2285. https://doi.org/10.1175/2009MWR2684.1

Foster, D. J., & Davy, R. D. (1988). *Global snow depth climatology, USAFETAC/TN-88/006*, (p. 48). Illinois: Scott Air Force Base.
Foster, J., Owe, M., & Rango, A. (1983). Snow cover and temperature relationships in North America and Eurasia. *Journal of Climate and Applied Meteorology*, *22*, 460–469.
Furtado, J. C., Cohen, J. L., Butler, A. H., Riddle, E. E., & Kumar, A. (2015). Eurasian snow cover variability and links to winter climate in the CMIP5 models. *Climate Dynamics*, *45*(9-10), 2591–2605. https://doi.org/10.1007/s00382-015-2494-4
Gnanadesikan, A., Dixon, K. W., Griffies, S. M., Balaji, V., Barreiro, M., Beesley, J. A., et al. (2006). GFDL's CM2 global coupled climate models. Part II: The baseline ocean simulation. *Journal of Climate*, *19*(5), 675–697. https://doi.org/10.1175/JCLI3630.1
Griffies, S.M., Harrison M.J., Pacanowski RC, Rosati A (2004). Technical guide to MOM4, GFDL Ocean Group Tech. Rep. 5, Geophys. Fluid Dyn. Lab., NOAA, Princeton, N. J. [Available at http://www.gfdl.noaa.gov/fms.]
Hahn, D. G., & Shukla, J. (1976). An apparent relationship between Eurasian snow cover and Indian monsoon rainfall. *Journal of the Atmospheric Sciences*, *33*(12), 2461–2462. https://doi.org/10.1175/1520-0469(1976)033<2461:AARBES>2.0.CO;2
Halder, S., & Dirmeyer, P. A. (2016). Relation of Eurasian snow cover and Indian summer monsoon rainfall: Importance of the delayed hydrological effect. *Journal of Climate*, *30*(4), 1273–1289. https://doi.org/10.1175/JCLI-D-16-0033.1
He, Q., Zuo, Z., Zhang, R., & Zhang, R. (2018). Seasonal prediction and predictability of Eurasian spring snow water equivalent in NCEP Climate Forecast System version 2 reforecasts. *Climate Dynamics*, *50*(1-2), 339–348. https://doi.org/10.1007/s00382-017-3611-3
He, Q., Zuo, Z. Y., Zhang, R. H., Yang, S., Wang, W. Q., Zhang, R. N., & Riddle, E. (2016). Prediction skill and predictability of Eurasian snow cover fraction in the NCEP Climate Forecast System version 2 reforecasts. *International Journal of Climatology*, *36*(12), 4071–4084. https://doi.org/10.1002/joc.4618
Huang, B., Shin, C. S., Shukla, J., Marx, L., Balmaseda, M., Halder, S., et al. (2017). Reforecasting the ENSO events in the past fifty-seven years (1958–2014). *Journal of Climate*, *30*(19), 7669–7693. https://doi.org/10.1175/JCLI-D-16-0642.1
Huang, B., Zhu, J., Marx, L., Wu, X., Kumar, A., Hu, Z. Z., et al. (2015). Climate drift of AMOC, North Atlantic salinity and arctic sea ice in CFSv2 decadal predictions. *Climate Dynamics*, *44*(1-2), 559–583. https://doi.org/10.1007/s00382-014-2395-y
Jhun, J.-G., & Lee, E.-J. (2004). A new East Asian winter monsoon indexand associated characteristics of the winter monsoon. *Journal of Climate*, *17*, 711–726.
Kim, H.-M., Webster, P. J., Curry, J. A., & Toma, V. (2012). Asian summer monsoon prediction in ECMWF system 4 and NCEP CFSv2 retrospective seasonal forecasts. *Climate Dynamics*, *39*(12), 2975–2991. https://doi.org/10.1007/s00382-012-1470-5
Koster, R. D., Mahanama, S. P. P., Yamada, T. J., Balsamo, G., Berg, A. A., Boisserie, M., et al. (2010). The contribution of land surface initialization to subseasonal forecast skill: First results from multi-model experiment. *Geophysical Research Letters*, *37*, L02402. https://doi.org/10.1029/2009GL041677
Kripalani, R. H., & Kulkarni, A. (1999). Climatology and variability of historical Soviet snow depth data: Some new perspectives in snow–Indian monsoon teleconnections. *Climate Dynamics*, *15*(6), 475–489. https://doi.org/10.1007/s003820050294
Li, Y., Wang, T., Zeng, Z., Peng, S., Lian, X., & Piao, S. (2016). Evaluating biases in simulated land surface albedo from CMIP5 global climate models. *Journal of Geophysical Research: Atmospheres*, *121*, 6178–6190. https://doi.org/10.1002/2016JD024774
Mahanama, S. P. P., Koster, R. D., Reichle, R. H., & Suarez, M. J. (2008). Impact of subsurface temperature variability on surface air temperature variability: An AGCM study. *Journal of Hydrometeorology*, *9*(4), 804–815. https://doi.org/10.1175/2008JHM949.1
Parthasarathy, B., & Yang, S. (1995). Relationships between regional Indian summer monsoon rainfall and Eurasian snow cover. *Advances in Atmospheric Sciences*, *12*(2), 143–150. https://doi.org/10.1007/BF02656828
Rodell, M., Houser, P. R., Jambor, U., Gottschalck, J., Mitchell, K., Meng, C.-J., et al. (2004). The global land data assimilation system. *Bulletin of the Seismological Society of America*, *85*(3), 381–394. https://doi.org/10.1175/BAMS-85-3-381
Roesch, A. (2006). Evaluation of surface albedo and snow cover in AR4 coupled climate models. *Journal of Geophysical Research*, *111*, D15111. https://doi.org/10.1029/2005JD006473
Saha, S., Moorthi, S., Pan, H. L., Wu, X., Wang, J., Nadiga, S., et al. (2010). The NCEP climate forecast system reanalysis. *Bulletin of the Seismological Society of America*, *91*(8), 1015–1058. https://doi.org/10.1175/2010BAMS3001.1
Saha, S., Moorthi, S., Wu, X., Wang, J., Nadiga, S., Patrick, T., et al. (2014). The NCEP Climate Forecast System Version 2. *Journal of Climate*, *27*(6), 2185–2208. https://doi.org/10.1175/JCLI-D-12-00823.1
Schultz, C., & Bregman, L. D. (1988). *Rand Corporation mean monthly global snow depth, Version 1*. Boulder, Colorado USA: NSIDC: National Snow and Ice Data Center. https://doi.org/10.7265/N57P8W9K
Seneviratne, S. I., Corti, T., Davin, E. L., Hirschi, M., Jaeger, E. B., Lehner, I., et al. (2010). Investigating soil moisture–climate interactions in a changing climate: A review. *Earth Science Reviews*, *99*(3-4), 125–161. https://doi.org/10.1016/j.earscirev.2010.02.004
Shukla, J., & Mintz, Y. (1982). Influence of land-surface evapotranspiration on the earth's climate. *Science*, *215*(4539), 1498–1501. https://doi.org/10.1126/science.215.4539.1498
Shukla, R. P., & Huang, B. (2015). Mean state and interannual variability of the Indian summer monsoon simulation by NCEP CFSv2. *Climate Dynamics*, *46*(11-12), 3845–3864. https://doi.org/10.1007/s00382-015-2808-6
Shukla, R. P., Huang, B., Dirmeyer, P. A., Kinter, J. L., Shin, C.-S., & Marx, L. (2019). Climatological influence of Eurasian winter surface condition on the Asian and Indo-Pacific summer circulation in the CFSv2 seasonal reforecasts. *International Journal of Climatology*, *39*(8), 3431–3453. https://doi.org/10.1002/joc.6029
Shukla, R. P., Huang, B., Marx, L., Kinter, J. L., & Shin, C.-S. (2017). Predictability and prediction of Indian summer monsoon by CFSv2: Implication of the initial shock effect. *Climate Dynamics*, *50*(1-2), 159–178. https://doi.org/10.1007/s00382-017-3594-0
Taylor, K. E., Stouffer, R. J., & Meehl, G. A. (2012). An overview of CMIP5 and the experiment design. *Bulletin of the Seismological Society of America*, *93*(4), 485–498. https://doi.org/10.1175/BAMS-D-11-00094.1
Towns, J., Cockerill, T., Dahan, M., Foster, I., Gaither, K., Grimshaw, A., et al. (2014). XSEDE: Accelerating scientific discovery. *Computing in Science & Engineering*, *16*(5), 62–74. https://doi.org/10.1109/MCSE.2014.80
Uppala, S. M., KÅllberg, P. W., Simmons, A. J., Andrae, U., Bechtold, V. D., Fiorino, M., et al. (2005). The ERA-40 re-analysis. *Quarterly Journal of the Royal Meteorological Society*, *131*(612), 2961–3012. https://doi.org/10.1256/qj.04.176
Wang, B., Ding, Q., Fu, X., Kang, I.-S., Shukla, J., & Doblas-Reyes, F. (2005). Fundamental challenge in simulation and prediction of summer monsoon rainfall. *Geophysical Research Letters*, *32*, L15711. https://doi.org/10.1029/2005GL022734
Wielicki, B. A., Barkstrom, B. R., Harrison, E. F., Lee, R. B. III, Louis Smith, G., & Cooper, J. E. (1996). Clouds and the Earth's Radiant Energy System (CERES): An earth observing system experiment. *Bulletin of the Seismological Society of America*, *77*(5), 853–868. https://doi.org/10.1175/1520-0477(1996)077<0853:CATERE>2.0.CO;2
Winton, M. (2000). A reformulated three-layer sea ice model. *Journal of Atmospheric and Oceanic Technology*, *17*(4), 525–531. https://doi.org/10.1175/1520-0426(2000)017<0525:ARTLSI>2.0.CO;2

Wu, B., Yang, K., & Zhang, R. (2009). Eurasian snow cover variability and its association with summer rainfall in China. *Advances in Atmospheric Sciences*, *26*(1), 31–44. https://doi.org/10.1007/s00376-009-0031-2

Wu, L. Y., & Zhang, J. Y. (2014). Strong subsurface soil temperature feedbacks on summer climate variability over the arid/semi-arid regions of East Asia. *Atmospheric Science Letters*, *15*(4), 307–313.

Xue, Y., Diallo, I., Li, W., David Neelin, J., Chu, P. C., Vasic, R., et al. (2018). Spring land surface and subsurface temperature anomalies and subsequent downstream late spring-summer droughts/floods in North America and East Asia. *Journal of Geophysical Research: Atmospheres*, *123*, 5001–5019. https://doi.org/10.1029/2017JD028246

Xue, Y., Oaida, C. M., Diallo, I., Neelin, J. D., Li, S., de Sales, F., et al. (2016). Spring land temperature anomalies in northwestern US and the summer drought over Southern Plains and adjacent areas. *Environmental Research Letters*, *11*(4), 044018. https://doi.org/10.1088/1748-9326/11/4/044018

Xue, Y., Sellers, P., Kinter, J. L., & Shukla, J. (1991). A simplified biosphere model for global climate studies. *Journal of Climate*, *4*(3), 345–364. https://doi.org/10.1175/1520-0442(1991)004<0345:ASBMFG>2.0.CO;2

Xue, Y., Vasic, R., Janjic, Z., Liu, Y. M., & Chu, P. C. (2012). The impact of spring subsurface soil temperature anomaly in the western U.S. on North American summer precipitation—A case study using regional climate model downscaling. *Journal of Geophysical Research*, *117*, D11103. https://doi.org/10.1029/2012JD017692

Yang, S., & Lau, K.-M. (1998). Influences of SST and ground wetness anomalies on the Asian summer monsoon. *Journal of Climate*, *11*(12), 3230–3246. https://doi.org/10.1175/1520-0442(1998)011<3230:IOSSTA>2.0.CO;2

Yasunari, Y., Kitoh, A., & Tokioka, T. (1991). Local and remote responses to excessive snow mass over Eurasia appearing in the northern spring and summer climate. *Journal of the Meteorological Society of Japan. Series II*, *69*(4), 473–487. https://doi.org/10.2151/jmsj1965.69.4_473

Zuo, Z. Y., Zhang, R. H., Wu, B. Y., & Rong, X. (2012). Decadal variability in springtime snow over Eurasia: Relation with circulation and possible influence on springtime rainfall over China. *International Journal of Climatology*, *32*(9), 1336–1345. https://doi.org/10.1002/joc.2355